Solid dispersion of β-lapachone in PVP K30 and PEG 6000 by spray drying technique

Klecia M. dos Santos[1] · Raquel de Melo Barbosa[1] · Lyghia Meirelles[1] · Fernanda Grace A. Vargas[1] ·
Antônio Claudio da Silva Lins[2] · Celso A. Camara[2] · Cicero F. S. Aragão[1] · Tulio Flavio de Lima Moura[1] ·
Fernanda Nervo Raffin[1]

Abstract

Beta-lapachone (βlap) is a naphthoquinone derived from Lapachol, a substance extracted from the Bignoniaceae family of trees, genus Tabebuia; found in the Northern and Northeastern regions of Brazil. βlap shows excellent pharmacological activity as an antiparasitic, antitumor, and anti-inflammatory drug, but its water solubility is low, which decreases its bio-availability. This work aims to evaluate the solubility and dissolution rate of βlap from solid dispersions obtained by the Spray Drying technique and compare them with the physical mixture (PM) of compounds. βlap solid dispersions were prepared with polyethylene glycol (PEG 6000) and polyvinylpyrrolidone (PVP K30) at 1: 2 (w/w) ratio and characterized by thermal analysis [differential scanning calorimetry (DSC)], X-ray powder diffraction (XRPD), Fourier transform infrared (FTIR), Scanning electron microscopy (SEM), solubility tests, dissolution profile assays and analyzed by mathematical models to link to the system properties. βlap/PVP solid dispersion provided a 15-fold increase in dissolution rate compared to pristine βlap in the first 5 min. The release constants obtained from Korsmeyer–Peppas and Weibull models demonstrate that βlap is released more rapidly from the PVP system produced by Spray Drying than by PM. The thermal analysis suggests that the βlap was successfully encapsulated into spherical shape and uniform size distribution microparticles produced by SD/PVP, as shown by the SEM technique. In addition, it afforded about 9-fold higher solubility than the free βlap. The results of DSC and XRD showed a tendency of the βlap crystallinity to decrease. FTIR showed intermolecular interaction between drug and polymer molecules (PVP and PEG). Thus, the results suggest that βlap/PVP-based solid dispersions can be successfully applied in pharmaceutical formulations.

Keywords Solid dispersion · Beta-lapachone · PEG 6000 · PVP K30 · Spray drying

Introduction

β-Lapachone (βlap) (Fig. 1) is antiparasitic, antitumor and anti-inflammatory drug with potential application in several areas of medicine [1–4]. However, its low water solubility limits systemic administration and clinical applications

in vivo. As a consequence, some methods have been purposed to increase the solubility and dissolution rate of βlap in aqueous systems like the use of cyclodextrins [5, 6], hydrogels [7], or liposomes [8].

The formation of solid dispersions (SD) is a simple and widely used process, consisting of a mixture of two or more components. In general, there are a hydrophilic (crystalline or amorphous) matrix and a hydrophobic drug, which may be molecularly dispersed or in the amorphous state [9, 10]. Among the hydrophilic polymers most used in the preparation of SD are polyethylene glycol (PEG) and polyvinylpyrrolidone (PVP K30) due to their ability to retard and inhibit drug crystallization, thus favoring increased dissolution rate [11, 12].

Solid dispersions are commonly prepared by melting, solvent, melt-solvent, spray drying, among others [13].
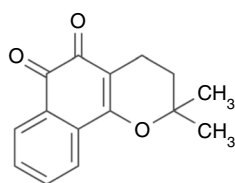
✉ Raquel de Melo Barbosa
m.g.barbosafernandes@gmail.com

Fernanda Nervo Raffin
feraffin@ufrnet.br

1 Department of Pharmacy, Federal University of Rio Grande do Norte, Natal, Rio Grande do Norte CEP 59012-570, Brazil

2 Department of Chemistry, Federal Rural University of Pernambuco, Recife, Pernambuco, Brazil

Fig. 1 The chemical structure of βlap

The spray drying technique is widely used to prepare SD. This technique consists on the dissolution of both drug and carrier in a suitable solvent, followed by the spray drying process to produce solid particles [14, 15]. Spray Drying is a method that allows the production of small spherical particles, allowing the increase in the particle's contact area in solution, which increases the dissolution rate of the drug and improves solubility [16, 17]. In this context, this work's aim is to prepare solid dispersions of βlap with different polymers (PEG and PVP) by the Spray Drying technique and evaluate drug solubility and dissolution rate in aqueous medium.

Materials and methods

Materials

βlap (7,8-benzo-2,2-dimethyl-3,4-dihydro-5,6-oxo-2H-chromene) was obtained by acid cyclization of lapachol isolated from the bark of the lapachol tree (*Tabebuia avellanedae*). Polyethylene glycol (PEG 6000), polyvinylpyrrolidone (PVP) type Kollidon K30 and ethanol were from Synth (São Paulo, Brazil). The dihydrogen and monohydrogen potassium phosphate salts were purchased by ISOFAR (Rio de Janeiro, Brazil). All reagents used were of analytical grade.

Methods

Production of physical mixtures (PMs) and microparticles

The PMs of βlap with two different polymers, PVP and PEG, were prepared in the ratio 1: 2 (w/w). Drug and polymer were weighed, mixed using mortar and pestle, and stored in a desiccator. The SD were prepared from binary blends of the βlap with PVP or PEG polymers in the ratio 1: 2 (w/w) in a water–ethanol solution (30/70%, v/v). Finally, the solutions were dried in the Dried Yamato Spray (Model ADL 311S, Yamato Scientific America Inc. California, USA), under the following operating conditions: inlet and outlet temperatures 75 °C and 60 °C, respectively, for the SD of βlap/PEG; inlet and outlet temperatures 145 °C and 80 °C, respectively, for the βlap/PVP solid dispersion; feed rate of 1.5 cm^3 min^{-1} and atomizing air pressure of 0.1 MPa, in both cases.

Physicochemical characterization

Thermal analysis The differential scanning calorimetry (DSC) analyses were performed using 4 mg of each sample in an alumina crucible with the temperature in the range of 25–525 °C at 10 °C min^{-1} heating rate. DSC assays were performed by TA Instruments SDTQ600 DSC equipment (New Castle, USA) under a nitrogen atmosphere and flow rate of 50 cm^3 min^{-1}.

Wide-angle X-ray diffraction X-ray powder diffraction (XRPD) was performed using a RIGAKU Mini Flex II diffractometer (Mini Flex II, Rigaku, Massachusetts, USA), Cu Kα radiation at 30 mA and 45 kV with scan rate of 5 min^{-1} and diffraction angles (2θ) in the range of 5–50°.

Fourier transform infrared (FTIR) FTIR spectra were obtained using a Shimadzu FTIR (Shimadzu, Kyoto, Japan, IRAffinity-1) spectrometer equipped with attenuated total reflectance (ATR) accessory. Spectra acquisition was performed in the spectral region from 4000 to 700 cm^{-1} using 4 cm^{-1} resolution and 32 scans for each spectrum.

Microscopic analyses Particle morphology and size results by scanning electron microscopy (SEM) were obtained by using a Shimadzu SSX-550 Superscan microscope (Kyoto, Japan). The samples were dispersed in double-sided carbon tape and coated with gold plating. The particle size distribution was obtained through SEM images based on the 200-particle count using the computer program ImageJ software (National Institute of Mental Health, Bethesda, Maryland, USA).

Solubility study βlap amounts equivalent to 10 mg of the drug from PMs and SDs were added to 10 cm^3 of potassium phosphate buffer solution at 0.020 mol L^{-1} (pH 7.4). All samples were kept under stirring in a homogenizer for 48 h at room temperature. The samples were filtered through a 250 mm sieve and analyzed in triplicate by UV spectrophotometry at 257 nm (Evolution 300, Thermo Scientific, USA) [18]. The same procedure was performed using 0.1 mol L^{-1} hydrochloric acid solution (pH 1.2).

Dissolution study To obtain the in vitro dissolution profiles of samples containing PVP, 10 mg of free βlap and equivalent amounts of PMs and SDs were added in 450 cm^3 of 0.020 mol L^{-1} potassium phosphate buffer solution (pH 7.4) and 0.1 mol L^{-1} hydrochloric acid solution (pH 1.2). The tests were performed in a SOTAX dissolution apparatus (model AT7, Switzerland) at 37 ± 0.5 °C using the paddle method at a rotation speed of 75 rpm. At predetermined time intervals (5, 10, 20, 30, 45, 90, and 120 min), the samples were collected, filtered, and diluted for drug

quantification. The assays were carried out in triplicate with the dissolution medium's replacement, and the drug content released was determined by UV spectrophotometry at 257 nm (Evolution 300, Thermo Scientific, USA).

Mathematical modeling of βlap release

The drug release profile is linked to the system properties and determines the amount of drug available for absorption. Aspects related to drug absorption, biodistribution, metabolism, and elimination (the so-called ADME processes) are of great relevance for predicting delivery systems' efficiency. The release profiles are influenced by the type of drug and matrix, polymorphic form, crystallinity, particle size, and drug solubility [19, 20].

The data were fitted using mathematical models to understand the release mechanism of βlap/PVP SD [21, 22]. The best-fitted models, Weibull and Korsmeyer–Peppas, were applied to the experimental release curves to characterize the mechanism of βlap release in the different formulations with PEG and PVP.

The Weibull model (Eq. 1), an empirical model, is based on drug cumulative fraction in solution and is considered as a function of time t.

$$\log\left[-\ln\left(1-m\right)\right] = \beta \; \log\left(t - \mathrm{Ti}\right) - \log\alpha \tag{1}$$

where "α" defines the timescale of the process, "Ti" is the time interval before the start of the release process (zero in most cases), and "β" is a shape parameter that characterizes the exponential curve, as follows: $\beta = 1$, first-order kinetics; $\beta > 1$, sigmoid; and $\beta < 1$, satellite [22].

The Korsmeyer–Peppas model, a semi-empirical model, exponentially correlates drug release with time (Eq. 2):

$$f_\mathrm{t} = at^\mathrm{n} \tag{2}$$

where "a" is a constant associated with the dosage form's structural and geometric characteristics. The "n" value is the release exponent that indicates the mechanism of drug release. The "ft" is the fractional drug release at time "t," being M_t/M_∞. "M_t" is the amount of drug released at time t, and M_∞ is the amount of drug released at the infinite time (corresponding to the total amount in the system).

According to the "n" value, it is possible to describe the release exponent by three different mechanisms: (1) $n < 0.43$—a classical Fickian diffusion mechanism; (2) $n > 0.85$—governed by Type II transport, involving polymer swelling and relaxation of the polymeric matrix, and (3) $0.43 > n > 0.85$—anomalous transport kinetics, combining the two diffusion mechanisms and Type II transport.

These two models explain how the drug is released from systems by determining parameter values (k, n, β) of each model and the linear correlation coefficient [23, 24].

Results and discussion

Figure 2a, b shows the DSC curves of βlap, polymers, PMs, and SDs. Endothermic peaks at approximately 156 °C and 66 °C are observed and correspond to βlap [6] and PEG's [10] melting temperature. Although PVP is an amorphous polymer with well-defined glass transition and absence of melting peak, no transition is observed in Fig. 2b, probably due to experimental conditions. The broad endothermic peak ranging from 45 to 142 °C is related to water loss due to its extremely hygroscopic nature [16].

The endothermic peak at 156 °C, attributed to the βlap melting, was suppressed by PM and SD of βlap/PEG in both samples, indicating βlap to be molecularly dispersed in these samples. In contrast, PEG's endothermic peak is maintained in both curves with shifts to lower temperatures (62 and 64 °C).

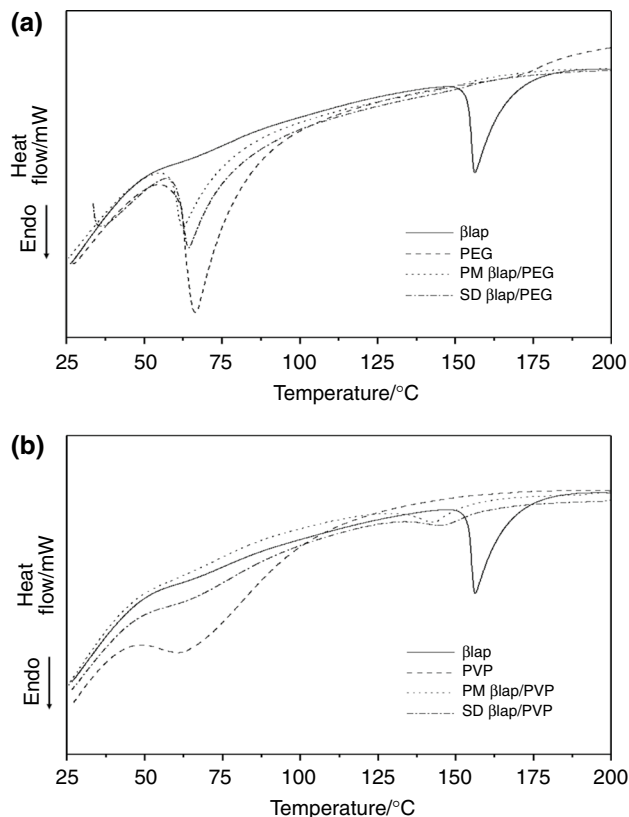On the other hand, PM and SD prepared with βlap/PVP exhibit a small endothermic peak of the drug, which shifts to

Fig. 2 DSC curves of βlap, PEG, PM, and SD prepared with PEG (**a**) and βlap, PVP, PM, and SD prepared with PVP (**b**)

142 and 145 °C, respectively. Further, the endothermic peak related to PVP tends to decrease in PM and SD. In general, the reduction or disappearance of the drug's endothermic peak can be attributed to the lack of crystallinity of the drug in the sample or solubility of the drug in the polymer, which suggests the amorphous nature of the materials obtained [25]. In a previous study [18] we observed similar results for SD at different βlap/PVP concentrations obtained by the solvent evaporation method. According to Vo & Lee, 2016, drug molecules can be distributed in the matrix, forming a solid dispersion in three different ways: (1) by the formation of eutectic systems (mixing two compounds) with a single melting point, which is lower than the melting point of individual components; (2) by the formation of solid solutions (substitutional, interstitial, or amorphous solid solutions); and (3) by the formation of microfine crystalline dispersions with drugs in the carrier matrix [26].
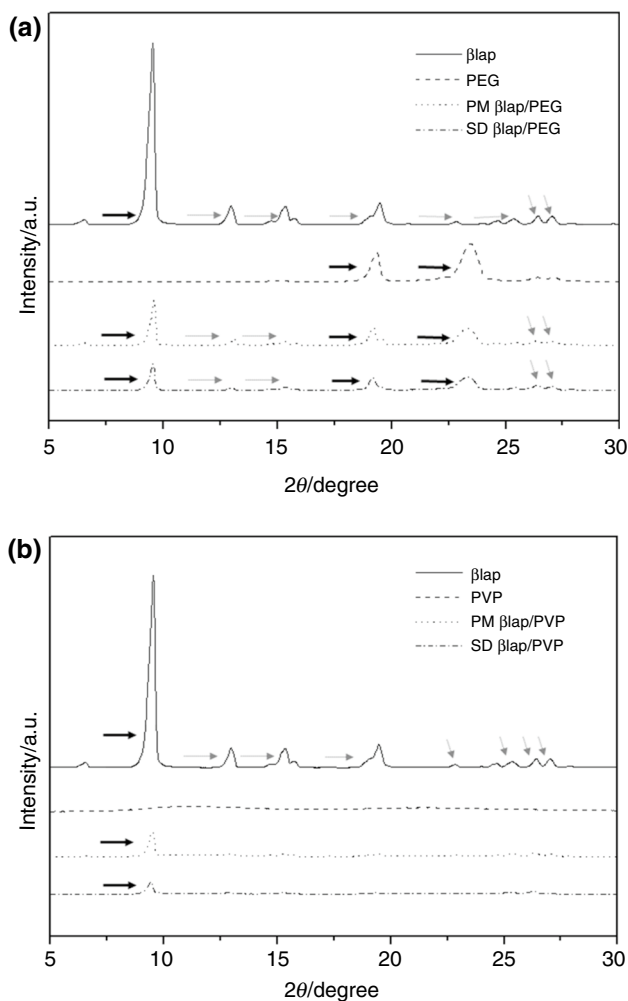
Diffractograms (XRPD) of pristine compounds (βlap, polymers), PMs, and SDs are presented in Fig. 3. Based on the results, βlap is present in its crystalline form, exhibiting the main peak at 9.5° and secondary peaks at 13.0°, 15.4°, 19.5°, 24.7°, 25.4°, 26.4°, and 27.0° [6]. The PEG has two main peaks at 19.3° and 23.5°, showing its semi-crystalline character [27]. The XRPD pattern of PVP indicates the absence of reflections due to its amorphous nature [28].

The PM of βlap/PEG and βlap/PVP shows similar diffraction patterns with the reduction of the drug crystalline state and superposition of the pristine materials' main reflections without new peaks or displacements, suggesting that no new interactions occurred. The samples obtained by SDs reveal a slightly lower relative intensity of the βlap peak than the PMs. This demonstrates a typical loss of drug crystallinity in the solid dispersions obtained, evidencing a tendency to the amorphous state as shown in the DSC curves (Fig. 2).
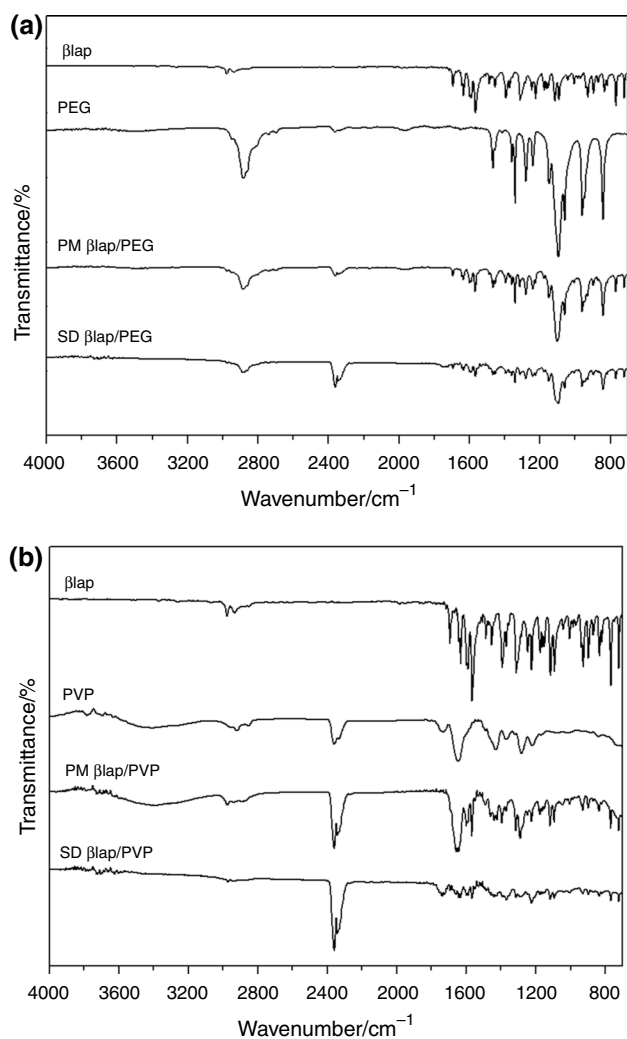

Fig. 3 XRPD patterns of βlap, PEG, PM, and SD prepared with PEG (**a**) and βlap, PVP, PM, and SD prepared with PVP (**b**)

Fig. 4 FTIR spectra of βlap, PEG, PM, and SD prepared with PEG (**a**) and βlap, PVP, PM, and SD prepared with PVP (**b**)

These results agree with studies found in the literature using PEG and PVP [29–31].

The FTIR spectra of βlap, polymers, PMs, and SDs, are shown in Fig. 4a, b. The spectra of βlap indicate the presence of characteristic absorption bands at 2978 cm^{-1} (C–H aromatic), 1694 cm^{-1} (C=O stretch), 1590, and 1567 cm^{-1} (C–C aromatic), and 1312 and 1115 cm^{-1} (C–O–C stretch) [6]. The bands ascribed to PEG were observed at 2882 cm^{-1} (C–H stretch) and 1095 cm^{-1} (C–O stretch) [32]. The FTIR spectra of PVP indicate the presence of a band at 3415 cm^{-1} (O–H stretch) associated with the presence of water, confirming the broad endothermic peak detected in the DSC curve. In addition, PVP shows other bands at 2919 cm^{-1} (C–H stretch), 1648 cm^{-1} (C=O stretch), and 1282 cm^{-1} (C–N stretch) [33].

In SD of βlap/PEG, the C–O band's relative intensity at around 1100 cm^{-1} and C=O stretches at 1694 cm^{-1} decreases compared to pristine βlap and polymer, indicating the hydrogen bond formation between hydroxyl groups of PEG and carbonyl groups of βlap, which are hydrogen bond acceptors. Regarding the PVP, the main fingerprint regions of polymer and βlap overlap, making it challenging to identify the displacements observed in PMs and SDs. However, relevant changes between the two binary products obtained are observed, such as the suppression of the CH stretch band of the βlap aromatic ring by 2978 cm^{-1}, simultaneous with the reduction of the intensity of the bands below 1800 cm^{-1}, including C=O (1648 cm^{-1}) referring to the polymer in SDs. Such changes suggest the formation of hydrogen bonds between chemical species, as the main mechanism of interaction in the SDs prepared from PEG and PVP, according to the literature [33–35].

Figure 5 shows SEM images of pristine material (Fig. 5a–c), PMs (Fig. 5d, e), and SDs (Fig. 5f, g). The
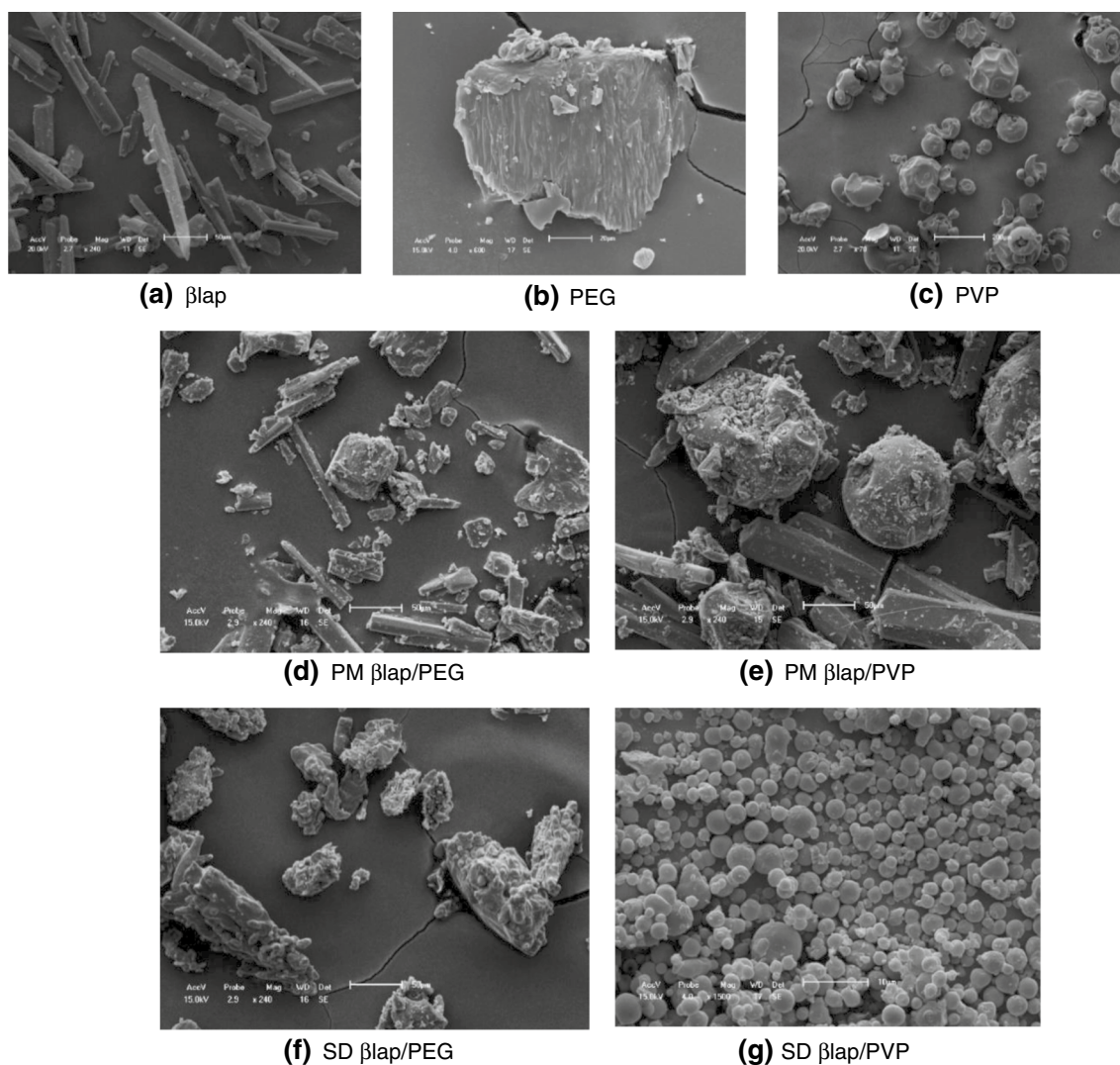
(a) βlap

(b) PEG

(c) PVP

(d) PM βlap/PEG

(e) PM βlap/PVP

(f) SD βlap/PEG

(g) SD βlap/PVP

Fig. 5 SEM image of βlap (**a**), PEG (**b**), PVP (**c**), PMs (**d** PM of βlap/PEG and **e** PM βlap/PVP) and SDs (**f** SD βlap/PEG and **g** SD of βlap/PVP)

micrographs reveal that the βlap (Fig. 5a) has a well-defined acicular crystal structure, PEG (Fig. 5b) with irregularly sized crystalline particles, whereas amorphous spherical particles form PVP (Fig. 5c). For PM of βlap/PEG and βlap/PVP (Fig. 5d, e respectively), the SEM images show the presence of drug crystals and particles of the polymers mixed [8, 31].

Figure 5f shows SEM images of the SD of βlap/PEG samples as agglomerates of non-spherical particles of varying sizes. Similar results were found in the literature using PEG SDs [36, 37]. In contrast, the SD of βlap/PVP shows the formation of well-defined spherical particles (Fig. 5g), indicating that the drug is incorporated in the polymer matrix [16].

Figure 6 shows the particle size distribution for the SD of βlap/PVP. The results indicate an average particle size of approximately 2.0 μm in diameter. The shape and the reduction of the particle size have an important influence on the solubility since they increase its contact area, making it more soluble [38, 39].

The results for the solubility study of βlap, PMs, and SDs is shown in Table 1. In both pH values, no increase in solubility of the PM and SD of βlap/PEG was observed compared to the drug. On the other hand, SD of βlap/PVP revealed a solubility approximately 7 and 9 times higher at pH 1.2 and 7.4, respectively. Further, for these samples, comparison verified that no significant difference exists between the results obtained in pH 1.2 and 7.4. This is because the chemical stability of the βlap in the aqueous medium is more significantly affected under basic
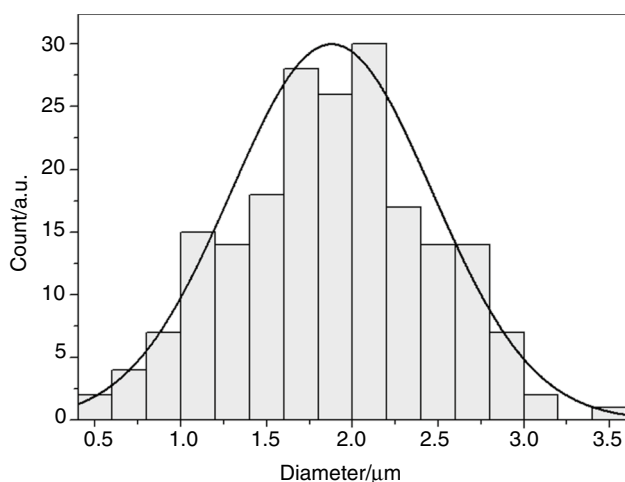
conditions than under acidic and neutral conditions since the drug undergoes alkaline hydrolysis [40].

The dissolution profiles and solubility at different pH values of βlap, PMs, and SDs are shown in Fig. 7a, b and Table 1, respectively. In fact, the dissolution tests were performed at physiological conditions (at 37 °C; 1.2 and 7.4 pH) for oral drug delivery. This study used different pHs to simulate acidic and neutral conditions (as found in stomach and small intestine, respectively) after a possible oral administration of the solid dispersion. At pH 7.4 a pronounced increase in the dissolution rate of βlap for SD is observed. However, within 5 min of the assay, SD of βlap/PVP revealed the drug's rapid release, indicating an approximately 19- and 15-fold increase in the dissolution rate at pH 1.2 and 7.4, respectively (Table 1).

The SD of βlap/PVP sample, at pH 7.4, reaches a maximum release of about 80% in 30 min, while the drug dissolves only 20% in this same time interval. Cunha-Filho et al. [41] obtained values around 89 and 92% of the dissolution efficiency at 30 min with βlap entrapped in Hydroxypropyl methylcellulose particles prepared using a solvent change precipitation process, the authors did not refer to the pH of the experiment. Cavalcanti et al. [8] encapsulated the βlap/hydroxypropyl-β-cyclodexdrin (HP β-CD) inclusion complex in liposomes and obtained drug release of about 70% in 24 h at pH 7.4.

The dissolution profile of SD βlap/PEG wasn't carried out due to the solubility data obtained showed low values. This was one of the determining factors for selecting the sample. In addition, the microphotographs obtained by SEM for SD βlap/PEG showed samples without defined morphology and aggregates of crystals of drugs and polymers. In contrast, the SD of βlap/PVP sample presented well-defined shapes in the order of few micrometers and a significant increase in the solubility of βlap in an aqueous medium.

This result shows the efficacy of the method proposed in this work since it shows a rapid drug release. The kinetic parameters obtained from in vitro release data applying the mathematical models are shown in Table 2 and Fig. 8a–d.

The drug release processes in vitro and in vivo can be evaluated using mathematical models extensively described in the literature. This work uses different mathematical models to determine the best mathematical fit and characterize the matrix's βlap release mechanism. Specifically, mathematical models also make it possible to determine parameters related to physical–chemical phenomena (such as the drug diffusion coefficient) and the drug dissolution rate. Further, the data
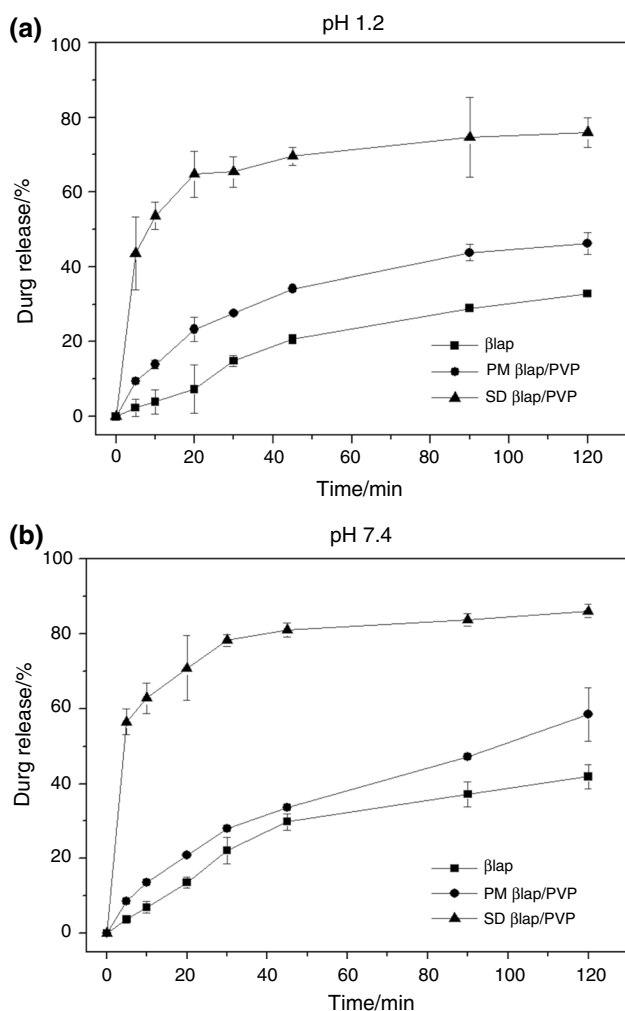

Fig. 6 The particle size distribution of SD of βlap/PVP

Table 1 Solubility of βlap at different pH values					
Solubility/mg mL^{-1}	βlap	PM βlap/PEG	SD βlap/PEG	PM βlap/PVP	SD βlap/PVP
HCl pH 1.2	0.052 ± 0.002	0.043 ± 0.001	0.048 ± 0.002	0.034 ± 0.001	$0.383 \pm 0,011$
Phosphate buffer pH 7.4	0.042 ± 0.003	0.039 ± 0.001	0.048 ± 0.001	0.037 ± 0.002	0.385 ± 0.005

Mean $\pm$ SD, $n = 3$

(a)

(b)

Fig. 7 The dissolution profiles of βlap, PM βlap/PVP, and SD βlap/PVP at 1.2 pH (**a**) and 7.4 pH (**b**)

Table 2 Kinetic model fitting for the drug release data

	pH 1.2		pH 7.4	
	PM βlap/ PVP	SD βlap/ PVP	PM βlap/ PVP	SD βlap/ PVP
Korsmeyer–Peppas				
n	0.462	0.170	0.591	0.136
k (min^{-1})	5.29	36.11	3.48	46.72
R^2	0.92	0.80	0.98	0.90
Weibull				
α	24.796	2.607	34.332	1.875
β	0.592	0.285	0.700	0.280
R^2	0.96	0.84	0.99	0.94

Release constants (k), correlation coefficient (r), and diffusion exponent (n) obtained by adjusting the curves of the release kinetics of samples in PMs and SDs with different pH and mass ratios

k: Release constant, R^2: Correlation coefficient, n: Diffusion exponent, α: Defines the time scale of the process, β: Indicates the mechanism of transport of the drug in the system

obtained can be translated as dissolution behaviors that can vary and pharmacokinetic parameters.

Weibull and Korsmeyer–Peppas' model show adjusted R^2 values between 0.80 and 0.99.

According to Table 2, the release exponent value ($n < 0.43$) extracted from the equations proposed by Korsmeyer–Peppas applied to the SD of βlap/PVP profiles at pH 1.2 and 7.4 suggests that release is governed by classical Fickian diffusion, as shown in all the formulations. Regarding release constants (k, from KP model) and the time scale of the process (α from W model), SD samples resemble PM samples in both pHs. Additionally, the values found for release constants k increase, and α decrease, demonstrating
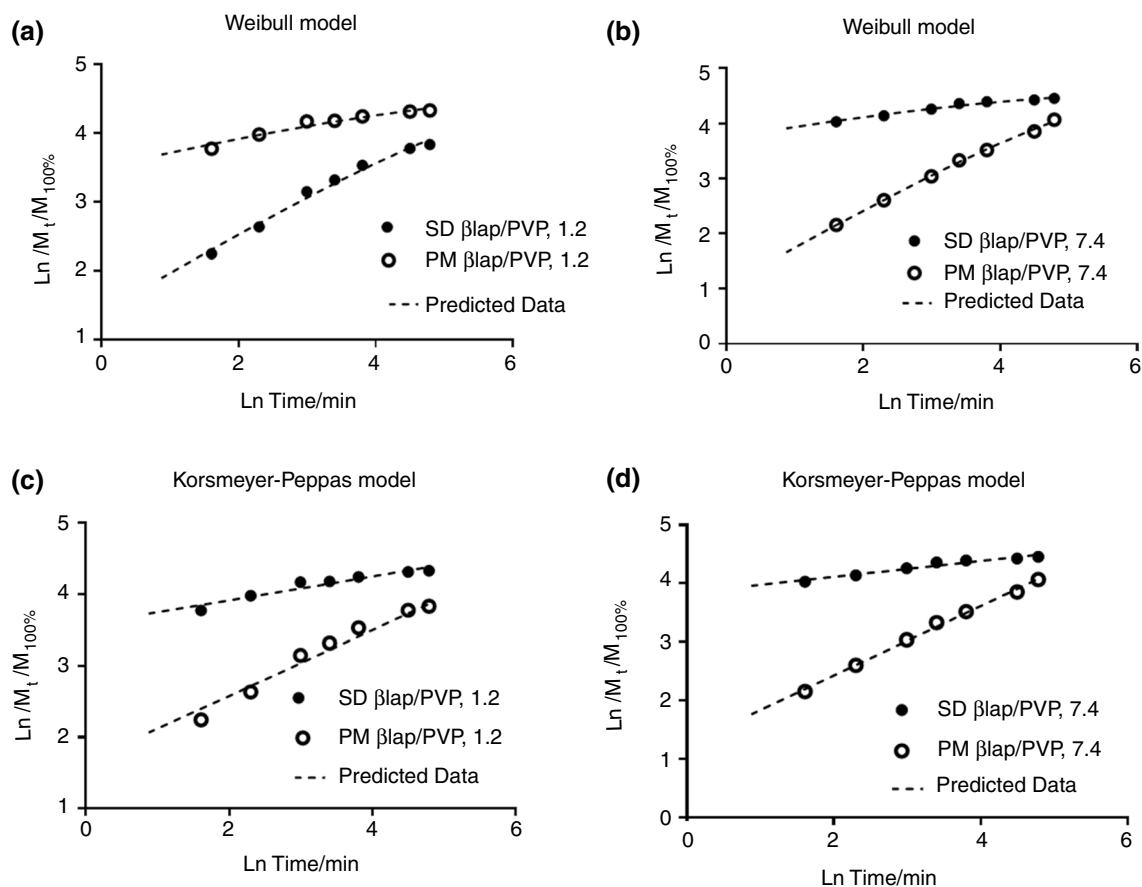
Fig. 8 Results of the PVP analyses containing βlap prepared by PM and SD at different pH values using the mathematical models of Weibull (**a** and **b**) and Korsmeyer–Peppas (**c** and **d**)

that βlap is released more rapidly from the PVP system produced by Spray Drying technique than in a simple PM.

However, in pH 1.2, the values of release constant *k* were lower than to SD samples in pH 7.4; this difference can be due to the viscous diffusion layer that significantly influenced the βlap inside the dispersing medium to impart slower diffusion of βlap.

Although many papers show that PVP forms a viscous diffusion layer in the dispersing medium, which can impart slower diffusion to βlap through this layer, SD produces amorphous compounds that favor βlap dissolution in aqueous medium at pH 7.4, i.e., crystallinity is reduced. Additionally, the particles' size and low polydispersity promoted by the Spray Drying technique significantly increase dissolution [42]. According to the Weibull equation, the *β* value indicates the mechanism of transport of the βlap in the slow kinetics system, as shown in all samples (Table 2).

Conclusions

In this work, solid dispersions, based on PEG and PVP, were prepared and characterized with great success using the spray drying technique. The results indicate that PVP greatly increases the solubility and rate of release of βlap in an aqueous medium. Also, samples with PVP show a rapid release of the drug and act as a carrier more efficiently than PEG. Based on these findings, we conclude that SD βlap/PVP can be applied as a satisfactory delivery system capable of improving the oral bioavailability of βlap.

References

1. Blanco E, Bey EA, Khemtong C, Yang SG, Setti-Guthi J, Chen H, Kessinger CW, Carnevale KA, Bornmann WG, Boothman DA, Gao J. βeta-lapachone micellar nanotherapeutics for non-small cell lung cancer therapy. Cancer Res. 2010. https://doi.org/10.1158/0008-5472.

2. Li LS, Bey EA, Dong Y, Meng J, Patra B, Yan J, Xie XJ, Brekken RA, Barnett CC, Bornmann WG, Gao J, Boothman DA. Modulating endogenous NQO1 levels identifies key regulatory mechanisms of action of beta-lapachone for pancreatic cancer therapy. Clin Cancer Res. 2011. https://doi.org/10.1158/1078-0432.CCR-10-1983.

3. Ríos-Luci C, Bonifazi EL, Léon LG, Montero JC, Burton G, Pandiella A, Misico RI, Padrón JM. β-lapachone analogs with enhanced antiproliferative activity. Eur J Med Chem. 2012. https://doi.org/10.1016/j.ejmech.2012.04.008.

4. Aires AL, Ximenes ECPA, Barbosa VX, Góes AJS, Souza VMO, Albuquerque MCPA. β-lapachone: a naphthoquinone with promising antischistosomal properties in mice. Phytomedicine. 2014. https://doi.org/10.1016/j.phymed.2013.08.012.

5. Nasongkla N, Wiedmann AF, Bruenin GA, Beman M, Ray D, Bommann WG, Boothman DA, Gao J. Enhancement of solubility and bioavailability of beta-lapachone using cyclodextrin inclusion complexes. Pharm Res. 2003. https://doi.org/10.1023/a:1026143519395.

6. Cunha-Filho MS, Dacunha-Marinho B, Torres-Labandeira JJ, Martinez-Pacheco R, Landin M. Characterization of β-lapachone and methylated β-cyclodextrin solid-state systems. AAPS PharmSciTech. 2007. https://doi.org/10.1208/pt0803060.

7. Díaz-Rodríguez P, Landin M. Smart design of intratumoral thermosensitive β-lapachone hydrogels by artificial neural networks. Int J Pharm. 2012. https://doi.org/10.1016/j.ijpharm.2012.05.008.

8. Cavalcanti IMF, Mendonça EAM, Lira MCB, Honrato SB, Camara CA, Amorim RVS, Filho JM, Rabello MM, Hernandes MZ, Ayala AP, Santos-Magalhães NS. The encapsulation of β-lapachone in 2-hydroxypropyl-β-cyclodextrin inclusion complex into liposomes: a physicochemical evaluation and molecular modeling approach. Eur J Pharm Sci. 2011. https://doi.org/10.1016/j.ejps.2011.08.011.

9. Baghel Shrawan, Cathcart Helen, O'Reilly Niall J. Polymeric amorphous solid dispersions: a review of amorphization, crystallization, stabilization, solid-state characterization, and aqueous solubilization of biopharmaceutical classification system class II drugs. J Pharm Sci. 2016. https://doi.org/10.1016/j.xphs.2015.10.008.

10. Lima AAN, Soares-Sobrinho JL, Silva JL, Côrrea-Júnior RAC, Lyra MAM, Santos FLA, Oliveira BG, Hernandes MZ, Rolim LA, Rolim-Neto PJ. The use of solid dispersion systems in hydrophilic carriers to increase benznidazole solubility. J Pharm Sci. 2011. https://doi.org/10.1002/jps.22436.

11. Kanaze FI, Kokkalou E, Niopas I, Georgarakis M, Stergiou A, Bikiaris D. Dissolution enhancement of flavonoids by solid dispersion in PVP and PEG matrixes: a comparative study. J Appl Polym Sci. 2006. https://doi.org/10.1002/app.24200.

12. Papadimitriou SA, Barmpalexis P, Karavas E, Bikiaris DN. Optimizing the ability of PVP/PEG mixtures to be used as appropriate carriers for the preparation of drug solid dispersions by melt mixing technique using artificial neural networks: I. Eur J Pharm Biopharm. 2012. https://doi.org/10.1016/j.ejpb.2012.06.003.

13. Tran P, Pyo Y, Kim D, Lee S, Kim J, Park J. Overview of the manufacturing methods of solid dispersion technology for improving the solubility of poorly water-soluble drugs and application to anticancer drugs. Pharmaceutics. 2019. https://doi.org/10.3390/pharmaceutics11030132.

14. Vicente J, Pinto J, Menezes J, Gaspar F. Fundamental analysis of particles formation of spray drying. Powder Technol. 2013. https://doi.org/10.1016/j.powtec.2013.06.038.

15. Singh A, Van den Mooter G. Spray drying formulation of amorphous solid dispersions. Adv Drug Deliv Rev. 2016. https://doi.org/10.1016/j.addr.2015.12.010.

16. Frizon F, Eloy JO, Donaduzzi CM, Mitsu ML, Marchetti JM. Dissolution rate enhancement of loratadine in polyvinylpyrrolidone K-30 solid dispersions by solvent methods. Powder Technol. 2013. https://doi.org/10.1016/j.powtec.2012.10.019.

17. Tran TH, Poudel BK, Marsini N, Woo JS, Choi H-G, Yong CS, Kim JO. Development of raloxifene-solid dispersion with improved oral bioavailability via spray-drying technique. Arch Pharm Res. 2013. https://doi.org/10.1007/s12272-013-0012-y.

18. dos Santos KM, Barbosa RM, Vargas FGA, Azevedo EP, Lins ACS, Camara CA, Aragão CFS, Moura TFL, Raffin FN. Development of solid dispersions of b-lapachone in PEG and PVP by solvent evaporation method. Drug development and industrial pharmacy. Drug Dev Ind Pharm. 2017. https://doi.org/10.1080/03639045.2017.1411942.

19. Censi R, Di Martino P. Polymorph impact on the bioavailability and stability of poorly soluble drugs. Molecules. 2015. https://doi.org/10.3390/molecules201018759.

20. Huang Y, Dai W. Fundamental aspects of solid dispersion technology for poorly soluble drugs. Acta Pharm Sin B. 2014. https://doi.org/10.1016/j.apsb.2013.11.001.

21. Korsmeyer RW, Gurny R, Doelker E, Buri P, Peppas NA. Mechanisms of solute release from porous hydrophilic polymers. Int J Pharm. 1983. https://doi.org/10.1016/0378-5173(83)90064-9.

22. Costa P, Lobo JMS. Modelling and comparison of dissolution profiles. Eur J Pharm Sci. 2001. https://doi.org/10.1016/S0928-0987(01)00095-1.

23. Grillo R, de Melo NF, de Araújo DR, de Paula E, Rosa AH, Fraceto LF. Polymeric alginate nanoparticles containing the local anesthetic bupivacaine Polymeric alginate nanoparticles containing the local anesthetic bupivacaine. J Drug Target. 2010. https://doi.org/10.3109/10611861003649738.

24. Marcato PD, Adami LF, Barbosa RM, Melo PS, Ferreira IR, de Paula L, Duran N, Seabra AB. Development of a sustained-release system for nitric oxide delivery using alginate/chitosan nanoparticles. Curr Nanosci. 2013. https://doi.org/10.2174/1573413713109010003.

25. Adeli E. A comparative evaluation between utilizing SAS supercritical fluid technique and solvent evaporation method in preparation od azithromycin solid dispersions for dissolution rate enhancement. J Supercrit Fluids. 2014. https://doi.org/10.1016/j.supflu.2013.12.020.

26. Vo CL, Park C, Lee B. Current trends and future perspectives of solid dispersions containing poorly water-soluble drugs. Eur J Pharm Biopharm. 2013. https://doi.org/10.1016/j.ejpb.2013.09.007.

27. Mirza S, Ki JHM, Miroshnyk I, Rantanen J, Christiansen L, Karjalainen M, Yliruus J. Understanding processing-induced phase transformations in erythromycin–PEG 6000 solid dispersions. J Pharm Sci. 2006. https://doi.org/10.1002/jps.20640.

28. Gorajana A, Rajendran A, Dua TP. Preparation, characterization and in vitro evaluation of nitrendipine solid dispersion. J Dispers Sci Technol. 2012. https://doi.org/10.1080/01932691.2011.579829.

29. Lee JH, Kim MJ, Yoon H, Shim CR, Ko HA, Cho SA, Lee D, Khang G. Enhanced dissolution rate of celecoxib using PVP and/or HPMC-based solid dispersions prepared by spray drying method. J Pharm Investig. 2013. https://doi.org/10.1007/s40005-013-0067-2.

30. Shahzad Y, Sohail S, Arshad MS, Hussain T, Shan SNH. Development of solid dispersions of artemisinin for transdermal delivery. Int J Pharm. 2013. https://doi.org/10.1016/j.ijpharm.2013.09.027.

31. Ng CL, Lee S-E, Lee J-K, Kim T-H, Jang WS, Choi J-S, Kim Y-H, Kim J-K, Park J-S. Solubilization and formulation of chrysosplenol

C in solid dispersion with hydrophilic carriers. Int J Pharm. 2016. https://doi.org/10.1016/j.ijpharm.2016.08.062.

32. Eloy JO, Marchetti JM. Solid dispersions containing ursolic acid in poloxamer 407 and PEG 6000: a comparative study of fusion and solvent methods. Powder Technol. 2014. https://doi.org/10.1016/j.powtec.2013.11.017.

33. Jahangiri A, Barzegar-Jalali M, Garjani A, Javadzadeh Y, Hamishenkar H, Asadpour-Zeynali K, Adibkia K. Evaluation of physicochemical properties and vivo efficiency of atorvastatin calcium/ezetimibe solid dispersion. Eur J Pharm Sci. 2016. https://doi.org/10.1016/j.ejps.2015.11.007.

34. Alves LDS, de La Roca Soares MF, Albuquerque CT, Silva ER, Vieira ACC, Fontes DAF, Figueiredo CBM, Sobrinho JLS, Neto PJR. Solid dispersion of efavirenz in PVP K30 by conventional solvent and kneading methods. Carbohydr: Polym; 2014. https://doi.org/10.1016/j.carbpol.2014.01.027.

35. Wu K, Li J, Wang W, Winstead DA. Formation and characterization of solid dispersions of piroxicam and polyvinylpyrrolidone using spray drying and precipitation with compressed antisolvent. J Pharm Sci. 2009. https://doi.org/10.1002/jps.

36. Corrigan DO, Healy AM, Corrigan OI. The effect of spray drying solutions of bendroflumethiazide/polyethylene glycol on the physicochemical properties of the resultant materials. Int J Pharm. 2003. https://doi.org/10.1016/s0378-5173(03)00338-7.

37. Janssens S, Armas HN, Roberts CJ, Van den Mooter G. Characterization of ternary solid dispersions of itraconazole, PEG 6000 and HPMC 2910 E5. J Pharm Sci. 2008. https://doi.org/10.1002/jps.21128.

38. Lage LM, Barichello JM, Lage DP, Mendonça DV, Carvalho AM, Rodrigues MR, Menezes-Souza D, Roatt BM, Alves RJ, Tavares CA, Coelho EA, Duarte MC. An 8-hydroxyquinoline-containing polymeric micelle system is effective for the treatment of murine tegumentary leishmaniasis. Parasitol Res. 2016. https://doi.org/10.1007/s00436-016-5181-4.

39. Vasconcelos T, Sarmento B, Costa P. Solid dispersions as strategy to improve oral bioavailability of poor water-soluble drugs. Drug Discov Today. 2007. https://doi.org/10.1016/j.drudis.2007.09.005.

40. Kim KH, Park S, Adhikary P, Cho H, Kang N, Jeong SH. Stability of β-lapachone upon exposure to various stress conditions: resultant efficacy and cytotoxicity. Chem Pharm Bull (Tokyo). 2016. https://doi.org/10.1248/cpb.c15-00706.

41. Cunha-Filho MS, Martínez-Pacheco R, Landín M. Dissolution rate enhancement of the novel antitumoral β-lapachone by solvent change precipitation of microparticles. Eur J Pharm Biopharm. 2008. https://doi.org/10.1016/j.ejpb.2008.02.014.

42. Karavas E, Georgarakis M, Docoslis A, et al. Combining SEM, TEM, and micro-Raman techniques to differentiate between the amorphous molecular level dispersions and nanodispersions of a poorly water-soluble drug within a polymer matrix. Int J Pharm. 2007. https://doi.org/10.1016/j.ijpharm.2007.03.037.